Power-efficient beam tracking during connected mode DRX in mmWave and sub-THz systems

Syed Hashim Ali Shah [1], Sundeep Rangan [2], and Sundar Aditya [2]

[1]NYU Wireless
[2]Affiliation not available

October 30, 2023

Abstract

Discontinuous reception (DRX), wherein a user equipment (UE) temporarily disables its receiver, is a critical power saving feature in modern cellular systems. DRX is likely to be aggressively used at mmWave and sub-THz frequencies due to the high front-end power consumption. A key challenge for DRX at these frequencies is blockage-induced link outages: A UE will likely need to track many directional links to ensure reliable multi-connectivity, thereby increasing the power consumption. In this paper, we explore reinforcement learning-based link tracking policies in connected mode DRX that reduce power consumption by tracking only a fraction of the available links, but without adversely affecting the outage and throughput performance. Through detailed, system level simulations at 28 GHz (5G) and 140 GHz (6G), we observe that even sub-optimal link tracking policies can achieve considerable power savings with relatively little degradation in outage and throughput performance, especially with digital beamforming at the UE. In particular, we show that it is feasible to reduce power consumption by 75% and still achieve up to 95% (80%) of the maximum throughput using digital beamforming at 28 GHz (140 GHz), subject to an outage probability of at most 1%.

Hosted file

`Power-efficient beam tracking during connected mode DRX in mmWave and sub-THz systems 2.zip` available at https://authorea.com/users/663405/articles/676082-power-efficient-beam-tracking-during-connected-mode-drx-in-mmwave-and-sub-thz-systems

Power-efficient beam tracking during connected mode DRX in mmWave and sub-THz systems

Syed Hashim Ali Shah, *Student Member, IEEE*, Sundar Aditya, *Member, IEEE* and Sundeep Rangan, *Fellow, IEEE*

Abstract

Discontinuous reception (DRX), wherein a user equipment (UE) temporarily disables its receiver, is a critical power saving feature in modern cellular systems. DRX is likely to be aggressively used at mmWave and sub-THz frequencies due to the high front-end power consumption. A key challenge for DRX at these frequencies is blockage-induced link outages: A UE will likely need to track many directional links to ensure reliable multi-connectivity, thereby increasing the power consumption. In this paper, we explore reinforcement learning-based link tracking policies in connected mode DRX that reduce power consumption by tracking only a fraction of the available links, but without adversely affecting the outage and throughput performance. Through detailed, system level simulations at 28 GHz (5G) and 140 GHz (6G), we observe that even sub-optimal link tracking policies can achieve considerable power savings with relatively little degradation in outage and throughput performance, especially with digital beamforming at the UE. In particular, we show that it is feasible to reduce power consumption by 75% and still achieve up to 95% (80%) of the maximum throughput using digital beamforming at 28 GHz $(140$ GHz$)$, subject to an outage probability of at most 1%.

Index Terms

Discontinuous reception (DRX), sub-terahertz (THz) communications, millimeter wave (mmWave) communications, Power-throughput trade-off, 5G, 6G, Beamforming, Multi-connectivity, Multiple-play

The authors are with NYU WIRELESS, Tandon School of Engineering, New York University, Brooklyn, NY 11201, USA (Email: {s.hashim, sundar.aditya, srangan}@nyu.edu).

This work was supported by the National Science Foundation under Grants 1302336, 1564142, and 1547332, NIST, SRC and the industrial affiliates of NYU WIRELESS. A part of this paper was presented at the International Workshop on Signal Processing Advances in Wireless Communications (SPAWC), 2019 held at Cannes, France [1].

multi-armed bandits (MP-MAB), Reinforcement learning, RFFE, Physical layer, Beam tracking, 3GPP, Blockage, Outage.

I. Introduction

A. Motivation

Mobile wireless communication in the mmWave and sub-THz bands enable multi-Gbps peak throughput, but at the cost of high power consumption in both the radio frequency front-end (RFFE) and digital baseband processing [2]–[4]. The high power consumption arises from the need to support a large number of antenna elements at very high sample rates, along with the relative inefficiency of RF components at high frequencies. Indeed, power consumption − particularly for mobile devices − is one of the most significant challenges facing 5G deployments today. For example, power estimates in [5] show that peak mobile RFFE power consumption for a typical 28 GHz device can exceed 1 W – a large portion of the total power budget. Recently, there has been significant interest in communication above 100 GHz, including the sub-THz and THz bands [6]–[9] Power consumption issues are likely to become even more acute in these frequencies. For example, a recent power estimate [10] showed that the UE receiver for a New Radio-like system at 140 GHz would require more than 30 times the power consumption of a receiver at 28 GHz, based on current device performances.

Discontinuous Reception (DRX) [11], [12], where a mobile device or UE temporarily disables its RFFE, is one of the most widely used tools to reduce power consumption in mobile devices. The DRX mechanism for the 5G new radio (NR) standards consists of three modes (states) [13], compared to legacy DRX with two states [14]. The three states are *Idle*, *Connected* and *Inactive*. In this work, we focus on connected mode DRX in which the UE is active and connected to the network.

Implementing DRX poses unique challenges in the mmWave and sub-THz bands [15]–[17]. Most importantly, mmWave systems communicate using narrow directional beams to overcome the high isotropic path loss [2]–[4]. Directional links need to be tracked to detect changes in the handset orientation, as well as link blockages – a key challenge in the mmWave bands [18]–[20]. In addition, mobile devices in mmWave cellular systems will likely require maintaining links to multiple cells for macro-diversity [21]. Thus, UEs will likely need to track links from multiple

directions from multiple cells. In connected mode DRX, this link tracking reduces the time a UE can turn off its RFFE, thereby creating trade-offs between power consumption, directional tracking and link reliability. For instance, if the UE decides to reduce link tracking to save power, how should the UE track the links so that the UE performance (e.g., outage probability, throughput, etc.) does not suffer severely? As we will show below, the number of beams to track and the rate of blockage increase in the bands above 100 GHz making the tradeoff even more important in the sub-THz regime.

In this paper, we address this question using a two-step approach, where, (i) given a constraint, K, which is related to the number of links to track by a scaling factor (and hence, acts as a power constraint), we represent the choice of links to track over time as the outcome a feasible policy for a multiple-play multi-armed bandit (MP-MAB) problem; and, (ii) given a policy for the MP-MAB problem in (i), we then identify the smallest K as the solution to an optimization problem that captures the power-performance trade-off.

Our contributions in this paper are:

1) For connected mode DRX in 3GPP NR, we estimate the UE RFFE power consumption at carrier frequencies of 28 and 140 GHz with analog and digital beamforming architectures, assuming system parameters taken from the 3GPP standard[1]. We show that the directional link tracking measurements are responsible for most of the power consumed in connected mode DRX, especially when the UE tracks all of the available links.
2) To reduce power consumption in connected mode DRX, we choose to track only a subset of the links (depending on K) at any time. We then cast the choice of links to track as the outcome of a policy for a MP-MAB problem.
3) Along with heuristic policy presented in our earlier work [1], we consider three classes of policies for the above MP-MAB problem: Thompson Sampling, Upper Confidence Bound (UCB), and ϵ-greedy. We then compare their strengths and weaknesses.
4) Given a policy for the MP-MAB problem in 3), we then identify the smallest K as the solution to an optimization problem that captures the power-performance trade-off.
5) We simulate the performance of different link tracking policies in (i) a 28 GHz system

[1]We use 3GPP NR as a benchmark, since it is the dominant standard for 5G systems. However, our DRX analysis would likely apply to other directional systems with intermittent transmissions as well.

similar in configuration to mmWave 5G NR deployments today [22]; and (ii) a hypothetical 140 GHz system[2]. At each of these frequencies, we compare the performance of the policies for both analog and digital beamforming at the UE. We find that at 28 GHz, digital beamforming can save more power (75%) and achieve a larger fraction (95%) of the maximum throughput than analog beamforming (50% power savings and 85% of the maximum achievable throughput), for an outage probability of at most 1%. The case for digital beamforming is even more compelling at 140 GHz, since none of our policies achieves an outage probability below 1% for analog beamforming, even in the absence of any constraint on the number of links that can be tracked. On the other hand, digital beamforming can save 75% power, while achieving 80% of the maximum throughput for an outage probability of at most 1%.

B. Related Work

DRX for LTE systems was studied in [23], while [15]–[17] focused on directional DRX for mmWave systems. These works concentrate on optimizing DRX parameters in the Radio Resource Control (RRC) layer (e.g., *ON Timer, DRX cycle,* etc.), whereas in this work, we focus on link tracking, which is a DRX issue at the physical (PHY) layer. Furthermore, [15]–[17] also focus on DRX performance in the *data arrival phase* (i.e., when the downlink data is arriving), through metrics like the queuing delay, and the wake-up latency. In this work, however, our primary interest is in the *pre-data arrival phase* (i.e., when no downlink data is arriving), where we are interested in the outage probability, since an outage in the pre-data arrival phase would lead to a loss of connectivity to the network. We also study DRX performance in the data arrival phase, however, with throughput as our performance metric.

DRX in a multi-connectivity setting is addressed in [24], but for the relatively simple scenario of dual connectivity in LTE systems, where the links are not prone to blocking-induced outages. However, at mmWave and sub-THz frequencies, where blockages are a major impediment, the degree of multi-connectivity is an important system parameter that impacts both the UE performance as well as power consumption, especially at sub-THz frequencies where the frequency and severity of blockages are likely to be greater than that at mmWave. To the best of our

[2]The 140 GHz band is the most likely sub-THz spectrum for future 6G systems [8].

knowledge, this power-performance trade-off and its implications for sub-THz UE beamforming architecture, which is a key theme of this paper, has not been studied previously.

C. Organization

This paper consists of seven sections. In Section II, we provide an overview of connected mode DRX, along with a model for DRX power consumption. In Section III, we capture the trade-off between power consumption and the measured channel quality in connected mode DRX by formulating the choice of links to track as the outcome of a policy for a MP-MAB problem. In Section IV, we present three sub-optimal, but effective, policies for the MP-MAB problem in Section III. The details of our simulation setup, modeling a 28 GHz 5G system and a hypothetical 140 GHz 6G system, are presented in Section V. Simulation results capturing the power-performance trade-off for the policies in Section IV are presented in Section VI, culminating in a discussion on the merits of digital beamforming at the UE, especially at sub-THz frequencies. Finally, Section VII concludes the paper with a summary.

D. Notation

$\mathbb{P}(.)$ denotes probability, $\mathbb{E}[.]$ the expectation operator, and $\mathcal{U}[a, b]$ represents a uniform random variable over $[a, b]$.

II. Analysis of 3GPP Connected Mode DRX

We first present an overview of connected mode DRX in the 3GPP NR standard [13]. Consider a UE situated within the coverage area of N_{cell} gNBs (base stations). Let N_{TX} and N_{RX} denote the number of antenna elements at the gNB and the UE, respectively. A key aspect of mmWave and sub-THz communications is the use of beamforming. We will assume that the gNB and the UE transmit and receive using finite beamforming codebooks [25], [26] for channel tracking and synchronization. Without loss of generality, we assume that the codebook size at the gNB and the UE equals N_{TX} and N_{RX}, respectively, which correspond to one codeword for each orthogonal spatial degree of freedom[3].

[3]A smaller codebook size reduces beam training overhead at the expense of beamforming resolution.

A. Connected Mode DRX concepts overview

Directional Tracking using Synchronization signals: We assume that the UE tracks the directional channel quality from the cells via the 5G NR synchronization signal blocks (SSBs) [13]. In the 5G NR system, each gNB periodically transmits a sequence of SSBs (known as an SSB *burst*) that sweep a set of TX directions [27], as illustrated in Fig. 1. Let T_{SSB} denote the duration of each SSB, T_{SS} the SSB burst period, and N_{SSB} the number of different TX directions swept in each SSB burst period, which depends on the TX codebook as shown in Fig. 1. To save power, we assume in Section III that in each SSB burst period, the UE chooses to track $K \leq N_{\mathrm{SSB}}$ SSB time slots (see Fig. 1, where $K = 4$ and N_{SSB} = 8). During other SSB time slots, the UE can go to sleep and save power by switching off its RFFE.

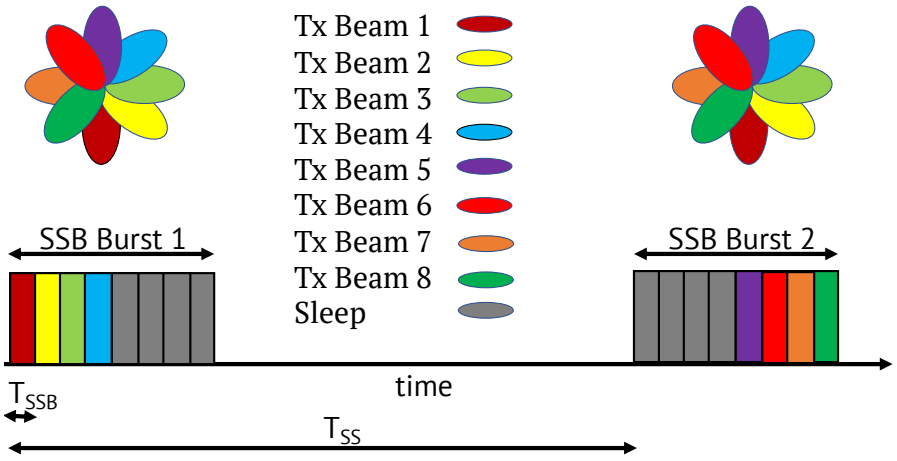

Fig. 1: Time line of a TX beam sweep using SSBs at the gNB, with $N_{\mathrm{SSB}} = 8$. The UE is awake for $K = 4$ SSB time slots in each SSB burst period. If the UE employs digital beamforming, then it can track along all the RX directions in each SSB time slot that it is awake for. With analog beamforming, however, the UE can only track along a single RX direction in a given SSB time slot.

Network Model with Carrier Aggregation: Resilience to blockage at mmWave frequencies necessitates macro-diversity, i.e., the UE must be connected to multiple cells [21], [28]. To this end, we assume that the UE is connected to all N_{cell} gNBs via *carrier aggregation*, a key feature in 3GPP systems that enables simultaneous connections to multiple cells [29]. The cells may operate in either different component carriers or within the same component carrier – the analysis for this paper is identical. We also assume that the cells are synchronized so that the SSB time slots from different cells are aligned.

B. Power Consumption in Connected Mode DRX

At a carrier frequency f_c with beamforming scheme $\mathrm{BF} \in \{\text{Analog, Digital}\}$, a UE in connected mode DRX, *not actively transmitting or receiving*, will need to periodically wake up for the following three events:

- Monitoring SSBs to measure the channel quality (beam measurements), which consumes $P_{\mathrm{BF}}^{f_c,\mathrm{BF}}$ units of power per SSB.
- Listening to assignments, which consumes $P_{\mathrm{LS}}^{f_c,\mathrm{BF}}$ units of power
- Beam reporting, which consumes $P_{\mathrm{BR}}^{f_c,\mathrm{BF}}$ units of power.

Among these, $P_{\mathrm{BF}}^{f_c,\mathrm{BF}}$ scales with the number of links that are tracked, while the other procedures have a fixed power cost. Hence, if the UE tracks a large number of links, $P_{\mathrm{BF}}^{f_c,\mathrm{BF}}$ could potentially become the dominant source of power consumption. The total power consumed by the UE RFFE, denoted by $P_{\mathrm{RX}}^{f_c,\mathrm{BF}}$, is given by:

$$P_{\mathrm{RX}}^{f_c,\mathrm{BF}} = P_{\mathrm{BM}}^{f_c,\mathrm{BF}} + P_{\mathrm{BR}}^{f_c,\mathrm{BF}} + P_{\mathrm{LS}}^{f_c,\mathrm{BF}}. \tag{1}$$

In Table I, we present estimates of $P_{\mathrm{BM}}^{f_c,\mathrm{BF}}$, $P_{\mathrm{BR}}^{f_c,\mathrm{BF}}$ and $P_{\mathrm{LS}}^{f_c,\mathrm{BF}}$, based on [10]. For further details, we refer the reader to Appendix A. Based on Table I, we make the following remarks:

Remark 1 (Digital beamforming with low-resolution ADCs)**.** *Conventionally, digital beamforming is believed to be more power hungry than analog beamforming due to the presence of multiple RF chains. However, a major source of the increased power consumption is the high resolution of the ADCs [30]. Recent works [5], [10] have shown that digital beamforming with low-resolution ADCs can significantly lower the RFFE power consumption with virtually no performance degradation. Throughout this paper, we assume digital beamforming with low-resolution (4-bit) ADCs.*

Remark 2. *Beam measurement on all the SSBs (i.e., tracking all the available links) is by far the largest source of power consumption in connected mode DRX, regardless of carrier frequency and the beamforming architecture.*

Remark 3 (Power consumption at 140 GHz)**.** *Digital beamforming at* 28 GHz *is slightly more power efficient than analog beamforming at* 28 GHz*, while both beamforming architectures have similar power consumption at* 140 GHz*. Relative to* 28 GHz*, the total power consumption at*

Task	**Fraction of time awake**		**Power Consumption Analog beamforming (mW)**		**Power Consumption Digital beamforming (mW)**	
	28 GHz	140 GHz	28 GHz	140 GHz	28 GHz	140 GHz
Beam measurement, 1 SSB $\left(P_{\mathrm{BM}}^{f_c,\mathrm{BF}}\right)$	0.0017	0.00089	0.39	6.05	0.17	6.12
Beam measurement, all SSBs $\left(N_{\mathrm{SSB}}.P_{\mathrm{BM}}^{f_c,\mathrm{BF}}\right)$	0.114	0.0571	24.96	774.4	10.88	783.36
Listening for assignments $\left(P_{\mathrm{LS}}^{f_c,\mathrm{BF}}\right)$	0.00625	0.00625	1.35	42.35	0.61	42.86
Beam reporting on PUCCH $\left(P_{\mathrm{BR}}^{f_c,\mathrm{BF}}\right)$	0.00357	0.00178	0.77	12.06	0.34	12.21

TABLE I: Estimated awake time and power consumption in DRX Connected Mode for parameters defined in Table VII

.

140 GHz *increases by a factor of 70 (35) for digital (analog) beamforming; thus, saving power at* 140 GHz *is crucial during link tracking.*

Remarks 2 and 3 motivate the need for the UE to reduce the number of links to track in order to save power. Thus, in the next section, we restrict the number of links that can be tracked at any time and then represent the choice of links to track over time as the outcome of a feasible policy for a multiple-play multi-armed bandit (MP-MAB) problem.

III. Problem Formulation

We index the SSB burst periods by $t = 0, 1, \ldots$, and let $\gamma_{ijk}(t)$ denote the measured channel quality (i.e., SNR) from cell $i = 1, \ldots N_{\text{cell}}$, in TX direction $j = 1, \ldots N_{\text{tx}}$, and RX direction $k = 1 \ldots N_{\text{rx}}$. The tensor γ_{ijk} depends on the UE motion, blocking, small-scale fading, and other

channel characteristics. Henceforth, we refer to the triplet (i, j, k) as a link. Let $\mathcal{A}(t)$, which we refer to as the *tracking set*, denote the set of links for which the UE chooses to measure the channel quality $\gamma_{ijk}(t)$ in SSB burst period t. The tracking set $\mathcal{A}(t)$ depends on: (a) the SSB time slots the UE chooses to track in the t-th SSB burst period, and (b) the RX directions the UE tracks. A larger $\mathcal{A}(t)$ increases the UE's probability of finding the best link. The trade-off, of course, is power consumption: tracking a larger number of links requires the UE to be awake longer.

In general, $\mathcal{A}(t)$ can be viewed as the outcome of a policy, $\pi(.)$, in the following manner:

$$\mathcal{A}(t) = \pi\left(\{\gamma_{ijk}[s] \in \mathcal{A}[s], s < t\}\right), \tag{2}$$

where, at each SSB burst period t, the choice of links to track is a function of past decisions. To reduce power consumption, we limit the number of SSB time slots that the UE is awake for in an SSB burst period to K $(1 \leq K \leq N_{\text{SSB}})$. The relationship between K and the cardinality of $\mathcal{A}(t)$, denoted by L, is as follows:

$$L := |\mathcal{A}(t)| = \begin{cases} K \times N_{\text{cell}}, & \text{for Analog beamforming,} \\ K \times N_{\text{cell}} \times N_{\text{RX}}, & \text{for Digital beamforming,} \end{cases} \tag{3}$$

where the scaling by N_{cell} is due to carrier aggregation. Hence, we restrict our attention to policies where the size of the tracking set is fixed for each t.

Given K, we choose $\mathcal{A}(t)$ to maximize the received SNR, $\gamma^{\pi}_{\max}(t)$, given by,

$$\gamma^{\pi}_{\max}(t) := \max_{(i,j,k)\in\mathcal{A}(t)} \gamma_{ijk}(t), \tag{4}$$

which can be categorized as a *multi-armed bandit (MAB)* problem in reinforcement learning (with $N_{\text{cell}} \times N_{\text{TX}} \times N_{\text{RX}}$ arms/links) with multiple (K) plays. The policy π aims to minimize the rate of growth of the cumulative regret $R^{\pi}(t)$, which is given by:

$$R^{\pi}(T) := \mathbb{E}\left[\sum_{t=1}^{T} \max_{(i,j,k)} \gamma_{ijk}(t)\right] - \mathbb{E}\left[\sum_{t=1}^{T} \gamma^{\pi}_{\max}(t)\right]. \tag{5}$$

In choosing $\mathcal{A}(t)$, a policy needs to trade-off between two competing requirements: *exploration* and *exploitation*. The latter, where the UE tracks the L links with the highest (measured) average SNR, helps to minimize the rate of growth of $R^{\pi}(.)$ in (5). However, the statistics of the links can change with time; hence, the UE needs to track sub-optimal links from time to time (i.e, exploration) to adapt to any changes in the L best links. Some well-known policies

in the reinforcement learning literature for solving multiple play MAB problems are: (i) the *ϵ-greedy algorithm* [31], (ii) *Thompson Sampling* [32], and (iii) the *Upper confidence bound (UCB) algorithm* [33]. We review them in the next section.

IV. Policies For Selective Link Probing in Connected Mode DRX

Before reviewing the policies, we first define some common quantities. Let $\mathcal{G}_n(t) := \{\gamma_n(s) : n \in \mathcal{A}[s],\ s \leq t\}$ denote the set of SNR values measured for the n-th link ($n = 1, \cdots, N_{\text{cell}} \times N_{\text{TX}} \times N_{\text{RX}}$) up to the t-th SSB burst period. Hence, $\hat{N}_n(t) := |\mathcal{G}_n(t)|$ denotes the number of times the n-th link has been included in the tracking set up to the t-th SSB burst period. Finally, let $\bar{\gamma}_n(t)$ denote the mean measured SNR of the n-th link up to the t-th SSB burst period (i.e., the sample mean of the elements of $\mathcal{G}_n(t)$).

A. Upper Confidence Bound (UCB) Algorithm

We adapt the policy presented in [33] for multiple play MAB problems. The UCB link tracking policy is summarized in Algorithm 1.

Remark 4. *The UCB link tracking policy in Algorithm 1 explores in the initialization stage. During the operation stage, (6) determines the SSB burst periods when exploration and exploitation take place*[4]*. A major drawback of the UCB policy is the requirement to measure all the links initially - in our simulation setup, for $K = 1$ (corresponding to the least power consumption) at 28 GHz with analog beamforming at the UE, this takes 10.2 s, which is orders of magnitude greater than the channel coherence time (around 21 ms)*[5]*. Hence, the channel statistics would have changed considerably by the time the UE decides to track (exploit) the best links found during the initial exploration.*

[4]As $\ln(t)$ increases in (6), a weak and therefore, infrequently tracked link (i.e., small $\bar{\gamma}_n(t)$ and $\hat{N}_n(t)$, respectively) is eventually included in the tracking set (i.e., exploration).

[5]For $K = 1$ with analog beamforming, the UE can measure only N_{cell} links (due to carrier aggregation) in one SSB burst period, out of a total of $N_{\text{cell}} \times N_{\text{TX}} \times N_{\text{RX}}$. Hence, the time taken for the initialization phase of Algorithm 4 equals $N_{\text{TX}} N_{\text{RX}} T_{\text{SSB}} = 10.2$ s at 28 GHz, for values chosen from Table VII. For a UE with an average velocity, v, of 0.5 m/s (human), the coherence time, $T_{\text{coh}} \approx c/(f_c v) \approx 21$ms [34].

Algorithm 1 UCB Link Tracking Policy

Data: $\gamma_{ijk}(t) : i = 1, \cdots, N_{\text{cell}}; j = 1, \cdots N_{\text{TX}}; k = 1, \cdots, N_{\text{RX}}; t = 1, \cdots, T\}$

Input : K

Initialization

$t \leftarrow 0$

for `t = 1 to` $N_{\text{cell}} \times N_{\text{TX}} \times N_{\text{RX}}/L$ **do**

- Measure L links : $\mathcal{A}(t) \cap \mathcal{A}(t-1) = \emptyset$

  {Make sure that all the beams have been measured at least once}
- Update $\bar{\gamma}_n(t)$ and $\hat{N}_n(t)$ accordingly
- $t \leftarrow t + 1$

end

Operation ($t > N_{\text{cell}} \times N_{\text{TX}} \times N_{\text{RX}}/L$)

- $t \leftarrow t + 1$
- Calculate:

$$\bar{\gamma}_n(t) + \sqrt{\frac{(L+1)\ln(t)}{\hat{N}_n(t)}}. \tag{6}$$

- Form the tracking set with L largest values in (6)
- Measure $\gamma^{\pi}_{\max}(t) = \max_{(i,j,k)\in\mathcal{A}(t)} \gamma_{ijk}(t)$.
- Update $\bar{\gamma}_n(t)$ and $\hat{N}_n(t)$ accordingly
- Go back to **Operation**

B. ϵ-Greedy Algorithm

Unlike the UCB algorithm, which has varying exploration and exploitation phases controlled by (6), the ϵ-greedy algorithm fixes the duration of these phases. Specifically, for $\epsilon \in (0, 1)$, the ϵ-greedy algorithm explores during $100\epsilon\%$ of the SSB burst periods and exploits during the remainder. The ϵ-greedy link tracking policy is summarized in Algorithm 2. The choice of ϵ is discussed in Section VI.

C. Thompson Sampling

In contrast to the previous policies, Thompson sampling adopts a Bayesian approach, where the average SNR of the n-th link is assumed to be a random variable, X_n. Assuming independence across links[6], let $f(X_n|\mathcal{G}_n(t))$ denote the posterior probability density function (pdf) of X_n,

[6]The SNRs of two or more links are, in general, not independent, due to correlated blocking.

Algorithm 2 ϵ-greedy Link Tracking Policy

Data: $\gamma_{ijk}(t) : i = 1, \cdots, N_{\text{cell}}; j = 1, \cdots N_{\text{TX}}; k = 1, \cdots, N_{\text{RX}}; t = 1, \cdots, T\}$

Input : K

Initialization

- $t \leftarrow 1$
- Uniformly and independently choose L links during the first SSB burst period {Initial Exploration}
- Calculate $\gamma^{\pi}_{\max}(t) = \max_{(i,j,k)\in\mathcal{A}(t)} \gamma_{ijk}(t)$.
- Update $\bar{\gamma}_n(t)$ and $\hat{N}_n(t)$ accordingly

Operation

- $t \leftarrow t + 1$
- Sample $u \sim \mathcal{U}[0, 1]$
- **if** $\epsilon < u$ **then**
  Form $\mathcal{A}(t)$ by uniformly and independently choosing L links {Exploration}
  else
  Form $\mathcal{A}(t)$ by using the largest L values of $\bar{\gamma}_n(t)$
  end
- Calculate $\gamma^{\pi}_{\max}(t) = \max_{(i,j,k)\in\mathcal{A}(t)} \gamma_{ijk}(t)$.
- Update $\bar{\gamma}_n(t)$ and $\hat{N}_n(t)$ accordingly
- Go back to **Operation**

given the measured values of γ_n up to the t-th SSB burst period. Starting from a prior pdf ζ_n, $f(X_n|\mathcal{G}_n(t))$ is updated every time the n-th link is included in the tracking set, using Bayes' rule. Thus, the policy aims to track the links with the L largest values of the posterior mean $\mathbb{E}[X_n|\mathcal{G}_n(t)]$.

The Thompson sampling based link tracking policy, adapted from [32][7], is presented in Algorithm 3. The performance of this policy depends on the choice of ζ_n and $f(X_n|\mathcal{G}_n(t))$. To evaluate the latter in a tractable manner, conjugate priors[8] are commonly assumed for ζ_n. The choice of distributions is discussed in Section VI-A.

[7]To the best of our knowledge, there exists no formal Thompson sampling policy for MP-MAB problems; hence, we adapt the conventional single play Thompson sampling policy for multiple plays.

[8]For the likelihood function, $f(\mathcal{G}_n|X_n)$, ζ_n is a conjugate prior if the posterior pdf, $f(X_n|\mathcal{G}_n)$, belongs to same family of distributions as ζ_n.

Algorithm 3 Thompson sampling based Link Tracking Policy

Data: $\gamma_{ijk}(t) : i = 1, \cdots, N_{\text{cell}}; j = 1, \cdots N_{\text{TX}}; k = 1, \cdots, N_{\text{RX}}; t = 1, \cdots, T\}$

Input : K, Prior pdf ζ_n $\forall n$

Initialization

- $t \leftarrow 0$
- Sample $x_n \sim \zeta_n,\ \forall n$
- Form $\mathcal{A}(t)$ by selecting the links corresponding to the L largest values among $\{x_n : n = 1, \cdots, N_{\text{cell}} \times N_{\text{TX}} \times N_{\text{RX}}\}$.

Operation

- Calculate $\gamma^{\pi}_{\max}(t) = \max_{(i,j,k)\in\mathcal{A}(t)} \gamma_{ijk}(t)$
- $t \leftarrow t + 1$
- Update $f(X_n|\mathcal{G}_n(t))$ $\forall n \in \mathcal{A}(t-1)$, using Bayes' rule [32].
- Sample $x_n \sim f(X_n|\mathcal{G}_n(t)),\ \forall n$
- Form $\mathcal{A}(t)$ by selecting the links corresponding to the L largest values among $\{x_n : n = 1, \cdots, N_{\text{cell}} \times N_{\text{TX}} \times N_{\text{RX}}\}$.
- Go back to **Operation**

D. $(L-1)$ *Round Robin Policy*

Finally, we consider a policy with one-step memory (i.e., $s = t-1$ in (2)) presented in [1]. For the current SSB burst period t, the policy retains the strongest link from $\mathcal{A}(t-1)$ and selects the other $L-1$ links independently and uniformly from the remaining links. We refer to this as $(L-1)$ *round robin policy*, which is summarized in Algorithm 4.

Remark 5. *In Algorithm 4, tracking the links in* $\hat{\mathcal{A}}(t)$ *can be viewed as exploration, while continuing to track* $m(t-1)$*, the strongest link from the previous SSB burst period, constitutes exploitation. Hence, the* $L-1$ *Round Robin policy resembles an* ϵ*-greedy policy with* $\epsilon = (L-1)/L$*. The* $(L-1)$ *Round Robin policy is also more memory efficient than the other three policies, since it does not maintain statistics for each link.*

V. Simulation Setup

Comprehensive link-level simulations are used to generate the channel trajectories at 28 GHz (5G) and 140 GHz (6G). Nine gNBs are deployed ($N_{\text{cell}} = 9$) in a 400 m $\times$ 400 m and the cell radius, r, of each gNB is 100 m. The heights of the gNBs and the UE are set to 10 m and

Algorithm 4 $(L-1)$ Round Robin Link Tracking Policy

Data: $\gamma_{ijk}(t) : i = 1, \cdots, N_{\text{cell}}; j = 1, \cdots N_{\text{TX}}; k = 1, \cdots, N_{\text{RX}}; t = 1, \cdots, T\}$

Input : K

Initialization

- At $t = 1$, construct $\mathcal{A}(t)$ for given K by uniformly and independently choosing L links to track
- Measure $\gamma^{\pi}_{\max}(t) = \max\limits_{(i,j,k)\in\mathcal{A}(t)} \gamma_{ijk}(t)\ \forall\ i$
- Let $m(t) := \arg\max\limits_{(i,j,k)\in\mathcal{A}(t)} \gamma^{\pi}_{ijk}(t)$ denote the strongest link in $\mathcal{A}(t)$
- $t \leftarrow t + 1$

Operation $(t > 1)$

- Form $\hat{\mathcal{A}}(t)$ by uniformly and independently choosing $L - 1$ links, excluding $m(t-1)$.
- $\mathcal{A}(t) = m(t-1) \cup \hat{\mathcal{A}}(t)$
- Measure $\gamma^{\pi}_{\max}(t) = \max\limits_{(i,j,k)\in\mathcal{A}(t)} \gamma_{ijk}(t)\ \forall\ i$
- Update $m(t)$
- $t \leftarrow t + 1$
- Go back to **Operation**

1.7 m, respectively, in accordance with the 3GPP 'UMi' specification [35]. At the start of each channel trajectory, the UE is dropped according to a two-dimensional uniform distribution that covers the grid.

Array Sizes and beamforming codebook design: In accordance with Table VII, a 4×2 (8×8) uniform planar array (UPA) is assumed at the UE and an 8×8 (16×16) UPA at the gNB for $f_c = 28$ (140) GHz. We assume a simple codebook, where the main lobes of the antenna patterns associated with each beamforming vector sweep through the whole sphere, equally spaced in both azimuth and elevation. We consider two similar antenna arrays at the UE for full 360 degree coverage like practical devices [36].

Blockers are placed using Poisson point process (PPP) [37] with blocker density $\lambda_b = 0.01$ m^{-2}. The blockers can be human or vehicular with equal probability. The dimensions and velocities of the blockers are chosen according to 3GPP modeling specifications [35] i.e., the height and width for a human (vehicular) blocker are 1.7 m $(1.5$ m$)$ and 0.3 m $(4.5$ m$)$, respectively. The magnitude of the velocities of human (vehicular) blockers are iid uniform between $[0, 3]$ $([0, 100])$ km/hr. The blockers are assumed to move in the xy plane.

We choose the Double Knife Edge Diffraction (DKED) model[9] for calculating blockage loss, since to the best of our knowledge, there is no parametric blockage model for 140 GHz. On the other hand, the DKED model is physics-based and holds for all frequencies. Moreover, measurement results in [39] show that the DKED model is within a few dB of the blockage loss at mmWave frequencies. Hence, we believe that the DKED model would provide a reasonably accurate estimate of the blockage loss at 140 GHz as well. The comparison of the blockage loss suffered due to a moving human blocker, according to the DKED model at sub-6 GHz (4G), 28 GHz (5G) and 140 GHz (possible 6G) is shown in Fig. 2. We see that the blockages are faster and deeper at sub-THz frequencies than in the mmWave regime.

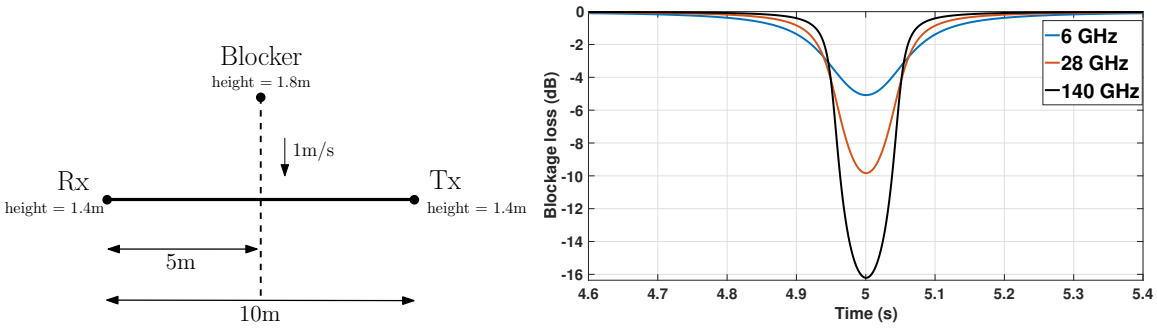

Fig. 2: Understanding the severity of blockages at higher frequencies. Left panel: A moving human blocker following 3GPP model parameters [35]. Right Panel: Blockage loss suffered by the signal due to double knife-edge diffraction for different frequencies.

Stationary Reflectors with density $\lambda_r = 0.01\ \mathrm{m}^{-2}$ are also deployed according to a PPP. We assume that the reflectors do not cause blockage. We form clusters of reflectors based on their proximity [40] and select up to N_{Cluster} clusters in increasing order of the gNB $\rightarrow$ cluster $\rightarrow$ UE path length [41], in addition to the line-of-sight path. The reflection loss suffered by the signal is taken to be 7 (10) dB at 28 (140) GHz [42][10].

Mobility: The reflectors are assumed to be static. The UE and blockers follow the random waypoint mobility model [43]. The UE and the human blockers have similar mobility characteristics, since their velocities are extracted from the same distribution; vehicular blockers have

[9]DKED is also known as *Blockage Model B* in 3GPP specifications [35] and is used in the METIS project [38].

[10]In general, the reflection loss depends on the material and the angle of incidence. For the sake of simplicity, we do not consider these effects.

Parameters	28 GHz	140 GHz	**Parameters**	28 GHz	140 GHz
Temperature	298 K		Cell radius, r	100 m	
Bandwidth	400 MHz	1.6 GHz	Blocker density	$0.01\ \mathrm{m}^{-2}$ [44]	
N_{TX}	64	256	Blocker height	1.4 m (Vehicular), 1.7 m (Human)	
N_{RX}	8	64	Blocker width	4.8 m (Vehicular), 0.3 m (Human)	
N_{cell}	9		Blocker speed distribution	$\mathcal{U}[0, 100]$ km/hr (Vehicular) $\mathcal{U}[0, 3]$ km/hr (Human)	
N_{Cluster}	4		Transmitted Power	23 dBm [45]	
UE height	1.7 m		Noise Figure	9 dB [46]	
gNB height	10 m		T_{SSB}	20 ms	
Reflection Loss	7 dB	10 dB	Scenario	UMi	

TABLE II: Values of different parameters for the generation of channel trajectories

a different velocity distribution. Let $x_t \in \mathbb{R}^2$ represent the position of an object during the t-th SSB burst period. At the next SSB burst period, the position is updated as follows:

$$x_{t+1} = x_t + \dot{x} T_{\mathrm{SSB}}, \tag{7}$$

where $\dot{x}$ is the velocity of the object. A destination is associated with every mobile object at the start of each simulation, which is changed when the object in question reaches the destination. The destination of the objects are restricted within the simulation grid.

We generate a total of 100 channel trajectories. For each trajectory, we simulate over 3000 SSB burst periods, with $T_{\mathrm{SSB}} = 20\mathrm{ms}$, amounting to a runtime of 60 s per trajectory. The list of parameters used to generate the simulation data is presented in Table II.

VI. Results and Discussion

In Sections VI-A and VI-B, we analyze the outage performance of the policies discussed in Section IV, for analog and digital beamforming at the UE, at 28 and 140 GHz. The purpose of this analysis is to quantify the amount of power the UE can potentially save, subject to satisfying an outage probability of at most 1%. The outage probability for a policy π, denoted by P^{π}_{out}, is defined as follows:

$$P^{\pi}_{\mathrm{out}} := \mathbb{P}(\gamma^{\pi}_{\mathrm{max}}(t) < \gamma_{\mathrm{tgt}}), \tag{8}$$

where γ_{tgt} is the minimum SNR required to communicate using MCS 0 - the lowest modulation and coding scheme (MCS). The value of γ_{tgt} can be obtained from (9) for $u = 0$.

A. *Parameter tuning for ϵ-greedy and Thompson sampling*

We begin by tuning the performance parameters for ϵ-greedy and Thompson sampling policies for each of the four scenarios to find the parameter values that yield the best results for our simulation setting.

1) Tuning ϵ: We proceed to find the best choice of ϵ for the four scenarios mentioned above in the interval $[0.01, 0.5]$. The choice of limits is motivated from a desire to have the policy explore more frequently than the initial exploration phase, but not so often that the best links are not exploited.

The P^{π}_{out} results for different ϵ values for all the cases are shown in Figs. 3 and 4. For the given set of ϵ, the ϵ_{tuned} values that yield the overall lowest P_{out} for each case are summarized in Table III.

Beamforming/ Frequency	**Analog/** 28 GHz	**Digital/** 28 GHz	**Analog/** 140 GHz	**Digital/** 140 GHz
ϵ_{tuned}	0.00125	0.01	0.00125	0.005

TABLE III: ϵ_{tuned} for different frequencies and beamforming schemes

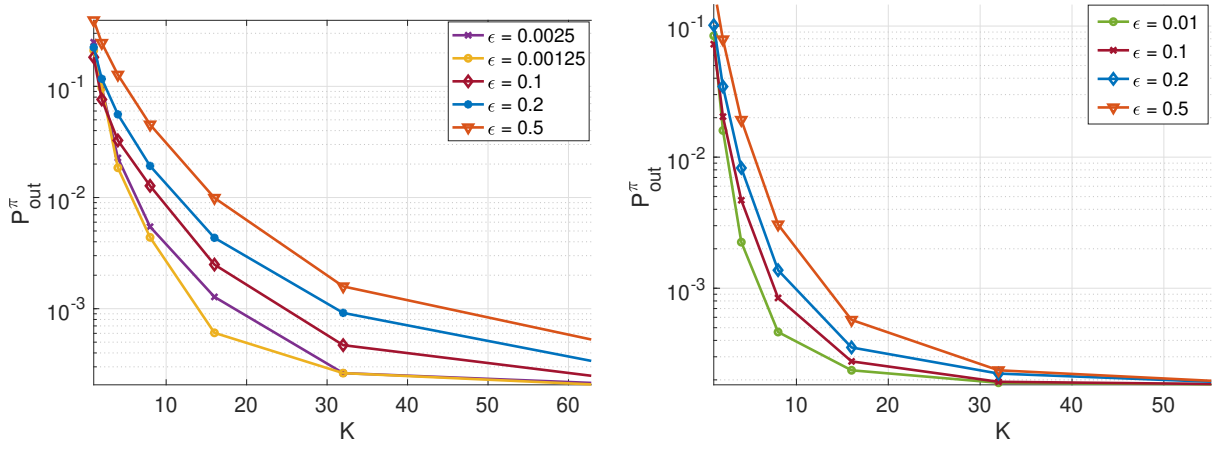

(a) Analog beamforming

(b) Digital beamforming

Fig. 3: P^{π}_{out} as a function of K for the ϵ-greedy link tracking policy for different values of ϵ at 28 GHz.

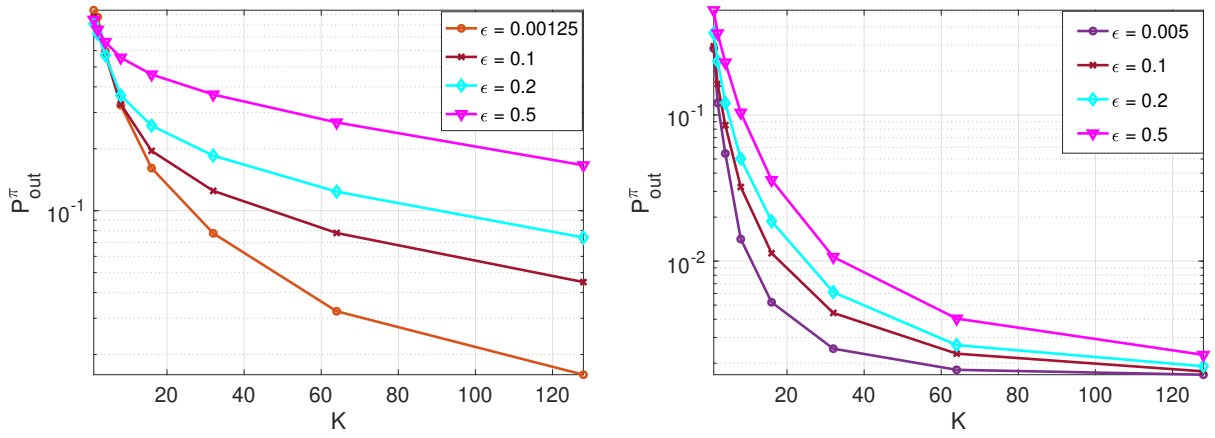

(a) Analog beamforming

(b) Digital beamforming

Fig. 4: P^{π}_{out} as a function of K for the ϵ-greedy link tracking policy for different values of ϵ at 140 GHz.

2) Choice of distributions for Thompson sampling: As discussed in Section IV, the performance of Thompson sampling depends on the choice of ζ_n and $f(X_n|\mathcal{G}_n(t))$ for the average link SNRs. We consider three distinct models from the exponential family for the likelihood function, $f(\mathcal{G}_n(t)|X_n)$, with each model corresponding to a conjugate prior choice for ζ_n:

(i) Gaussian ζ_n, assuming Gaussian $f(\mathcal{G}_n(t)|X_n)$,

(ii) Gamma ζ_n, assuming exponential $f(\mathcal{G}_n(t)|X_n)$, and

(iii) Beta ζ_n: Instead of the average SNR, the outage probability of the individual links can also be used to determine the tracking set. Let $\theta_n \in (0,1)$ denote the outage probability of the n-th link. Given $\mathcal{G}_n(t)$, let $\mathbf{g}_n(t)$ denote the binary vector (of size $\hat{N}_n(t)$) obtained by mapping the measured SNRs above and below γ_{tgt} to 0 and 1, respectively. Thus, $\mathbf{g}_n(t)$ captures the instances (up to the t-th SSB burst period) when the n-th link is *measured* to be in outage. Since $\mathbf{g}_n(t)$ is a sufficient statistic for estimating θ_n, Algorithm 3 can be used to determine $\mathcal{A}(t)$ by replacing X_n with θ_n and $\mathcal{G}_n(t)$ with $\mathbf{g}_n(t)$, respectively. As $\mathbf{g}_n(t)$ takes values in $\{0,1\}$, we assume Bernoulli $f(\mathbf{g}_n(t)|\theta_n(t))$, leading to Beta ζ_n.

Since the above priors are completely specified by two parameters, updating the posterior distribution $f(X_n|\mathcal{G}_n(t))$ in Algorithm 3 reduces to a simple update rule for the parameters at each t [32].

We denote ζ_{tuned} as the best prior distribution from the choices of distributions mentioned

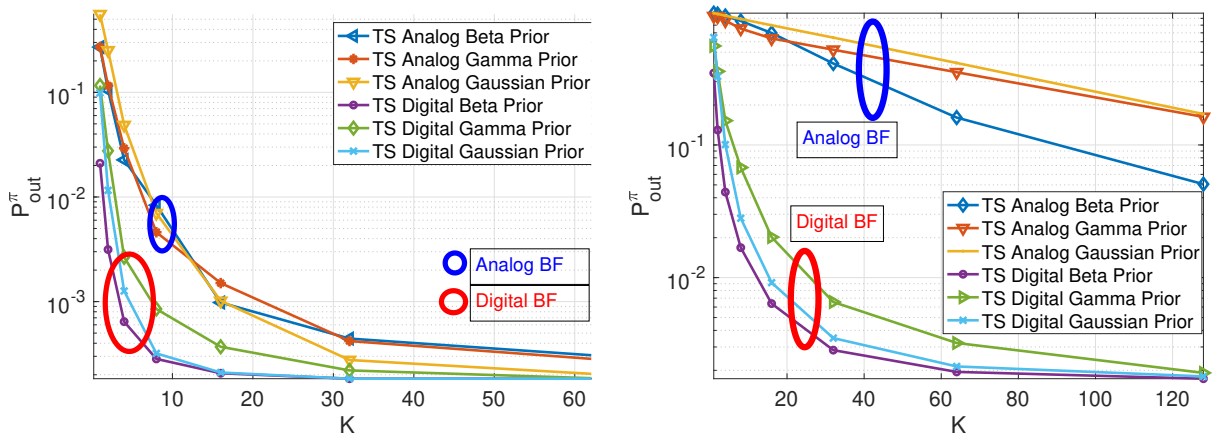

(a) 28 GHz

(b) 140 GHz

Fig. 5: P^{π}_{out} as a function of K for the Thompson sampling (TS) link tracking policy for different prior distributions ζ at 28 and 140 GHz with analog and digital beamforming.

above. The results for different ζ for all four scenarios can be observed in Fig. 5. The values of ζ_{tuned} that provide the overall best outage performance are summarized in Table IV.

Beamforming/ Frequency	**Analog/** 28 GHz	**Digital/** 28 GHz	**Analog/** 140 GHz	**Digital/** 140 GHz
ζ_{tuned}	Gaussian Prior	Beta Prior	Beta Prior	Beta Prior

TABLE IV: ζ_{tuned} for different frequencies and beamforming schemes

B. Outage Performance of Policies

After tuning the parameters of the ϵ-greedy and Thompson sampling policies, we proceed to compare the outage performance of all the policies in connected mode DRX with respect to the best possible performance, denoted by "Genie", where the UE knows apriori the link with the highest SNR.

At 28 GHz with analog beamforming, we see from Fig. 6a that $K = 8$, which translates to the UE being awake for only 12.5% of the time during an SSB burst period, results in an outage probability of less than 1% for three of the four policies (except $L-1$ Round Robin). For digital beamforming, the power savings are greater as $K = 4$ (i.e., 6.25% awake time) is sufficient to achieve the same outage performance for all the policies (see Fig. 6b).

At 140 GHz, we see from Fig. 7 that the performance gap between analog and digital beamforming is very large, compared to 28 GHz. In particular, for analog beamforming with $K = 128$ (i.e., the UE is awake for the whole SSB burst period), the outage probability is still more than 1% for all the link tracking policies (Fig. 7a) . On the other hand, for digital beamforming, $K = 16$ (i.e., the UE can sleep for 87.5% of the time during an SSB burst period) results in an outage probability of less than 1% for three of the four policies (except $L-1$ Round Robin, see Fig. 7b). The performance degradation for analog beamforming is due to a larger search space at 140 GHz, coupled with the non-stationarity of the link SNRs, which render it difficult for MP-MAB policies that typically assume stationarity to track (exploit) the strongest links[11]. This observation makes a compelling case for deploying fully digital beamforming architectures for possible 6G networks.

The best performing policy in our simulations for each case, in terms of the smallest sum of P^{π}_{out} across K, is reported in Table V. As a concluding remark, we emphasize that we make no broad claims on the *optimality* of any policy with respect to a given metric; rather, we view the performance of these sub-optimal, *off-the-shelf* policies as benchmarks that can be expected to be met by a link selection policy specifically tailored for connected mode DRX operation. The

[11]Bandit algorithms can be effective in tracking non-stationary processes [47], provided the statistics of the process do not evolve faster than the time it takes to learn them.

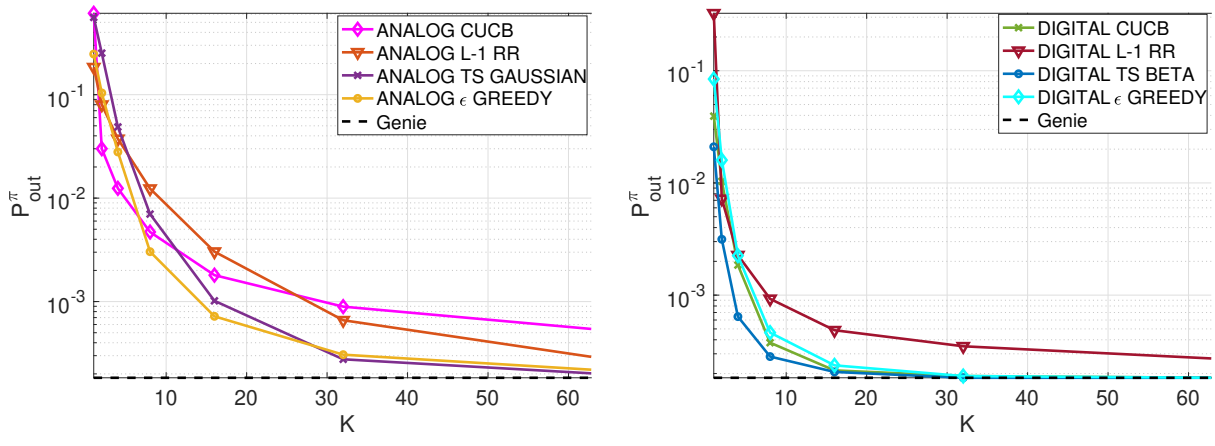

(a) Analog beamforming

(b) Digital beamforming

Fig. 6: P^{π}_{out} as a function of K for different policies at 28 GHz.

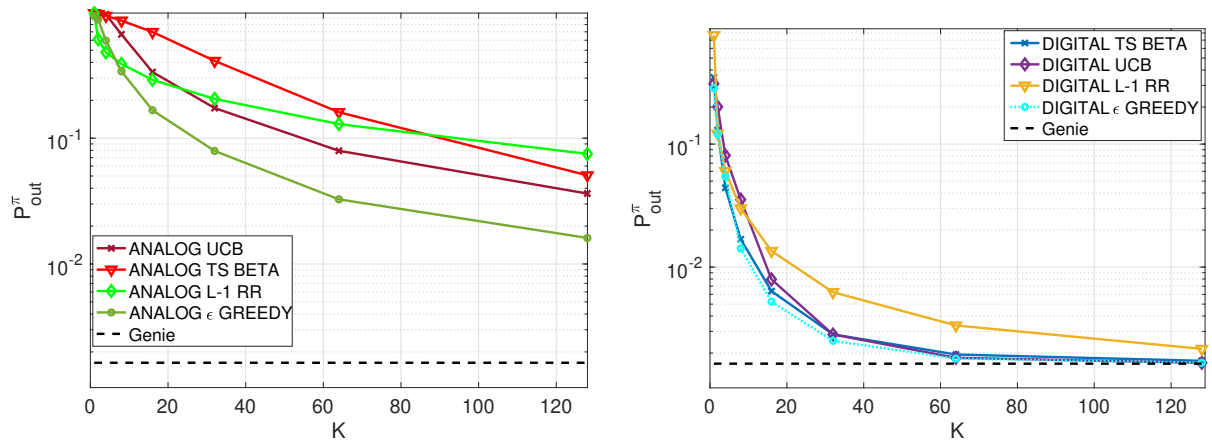

(a) Analog beamforming

(b) Digital beamforming

Fig. 7: P^{π}_{out} as a function of K for different policies at 140 GHz.

design of such a policy, along with provable performance guarantees, is left for future work.

Beamforming/ Frequency	**Analog/** 28 GHz	**Digital/** 28 GHz	**Analog/** 140 GHz	**Digital/** 140 GHz
Best Policy	ϵ-greedy	Thompson sampling	ϵ-greedy	ϵ-greedy

TABLE V: Best performing policies in our simulations.

C. Power vs. Throughput Trade-off

In this section, we formulate an optimization problem that captures the trade-off between the power consumed by UE and throughput. We use the spectral efficiency η, of the MCS levels to map $\gamma^{\pi}_{\max}$ to throughput from [48, Table 1]. We consider MCS 0-28 ($u = 0 \ldots 28$) for downlink communications from 3GPP standard. Let η_u be the spectral efficiency of u-th MCS. Let $\hat{\gamma}_u$ denote the minimum SNR need to decode MCS u, given by:

$$\widehat{\gamma}_u = 10 \log_{10}(2^{\eta_u} - 1) + \Delta. \tag{9}$$

The loss factor Δ, in dB, is a measure of how far the system is operating from Shannon capacity. The value of $\Delta = 3$ dB is in accordance with [5], [41], [49]. We define p_{uK} as the probability that MCS u is supported when the UE is awake for K SSBs i.e.,

$$p_{uK} = \mathbb{P}(\gamma^{\pi}_{\max} \geq \widehat{\gamma}_u). \tag{10}$$

p_{uK} is measured for $K = [1, 2, 4, 8, 16, 32, 64]$ SSBs at 28 GHz and for $K = [1, 2, 4, 8, 16, 32, 64, 128]$ at 140 GHz with the best policies for each case as per Table V. For a fixed u (i.e., fixed throughput), both the UE power consumption as well as p_{uK} increases with increasing K, as there is a greater chance that the UE can discover a better link if it awake for longer. On the other hand, for a fixed K, as u increases, the spectral efficiency and hence, the throughput increases as well but p_{uK} decreases because the minimum SNR required to decode a higher MCS is greater, thereby increasing the threshold in (10). Matrix visualizations of p_{uK}, reflecting these observations are shown in Figs. 8 and 9.

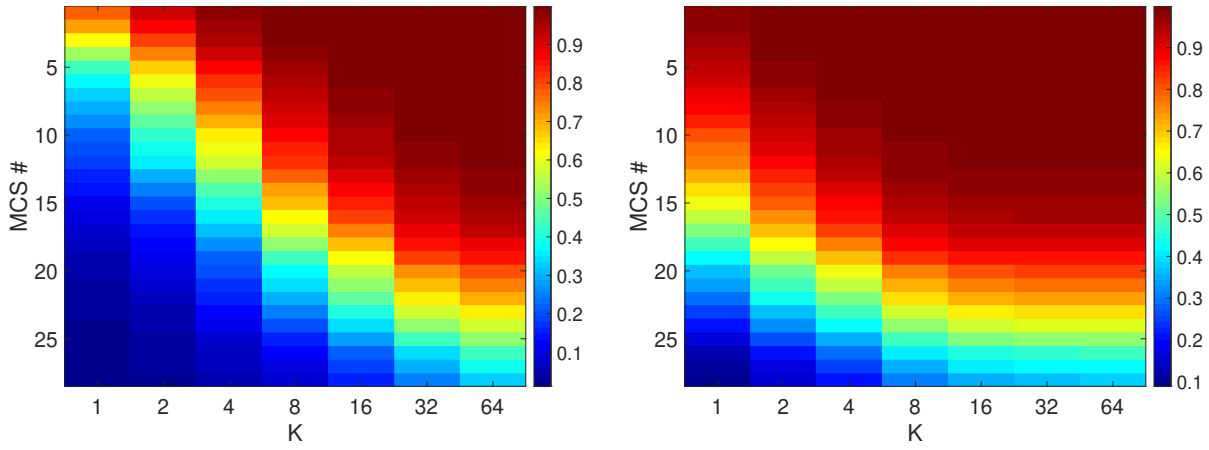

(a) Analog beamforming

(b) Digital beamforming

Fig. 8: Matrix visualization of p_{uK} for analog and digital beamforming at 28 GHz

From p_{uK}, the expected spectral efficiency $\mathbb{E}[\eta_{uK}]$ for MCS u and awake time K can simply be calculated as:

$$\mathbb{E}[\eta_{uK}] = p_{uK}\eta_u. \tag{11}$$

We capture the power-throughput trade-off in the following optimization problem:

$$\arg\max_{u,K} \ \mathbb{E}[\eta_{uK}] - \delta K \tag{12}$$

$$\text{s.t. } p_{uK} \geq P_o. \tag{13}$$

In (12), $\delta > 0$ is a tunable parameter that can be used to penalize power consumption, e.g., for a cellphone operating in low-power mode, a large δ is appropriate, whereas for a fully charged device anticipating high throughput traffic, a low δ may be suitable. The constraint (13) ensures that the optimal solution supports the chosen MCS with a minimum probability of P_o.

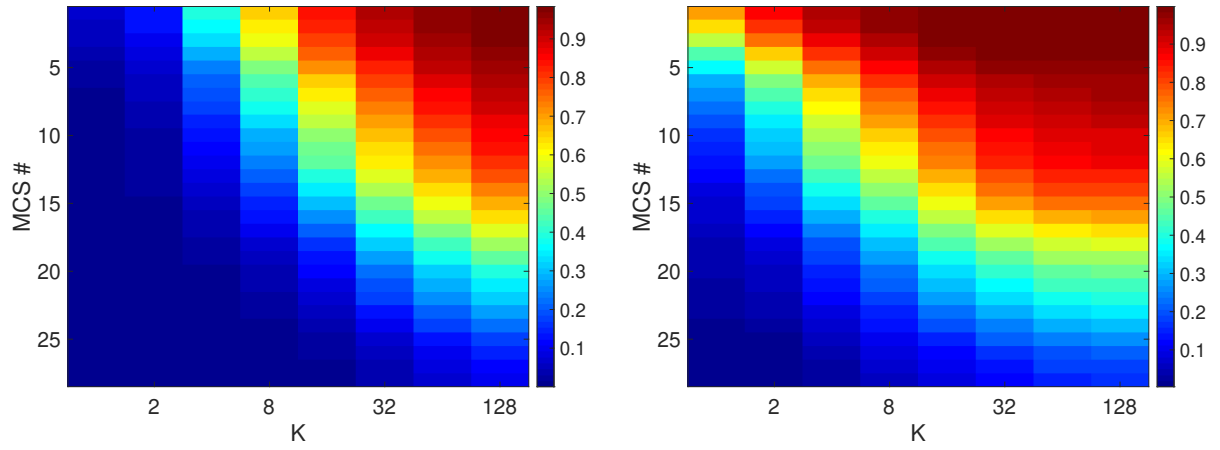

(a) Analog beamforming

(b) Digital beamforming

Fig. 9: Matrix visualization of p_{uK} for analog and digital beamforming at 140 GHz

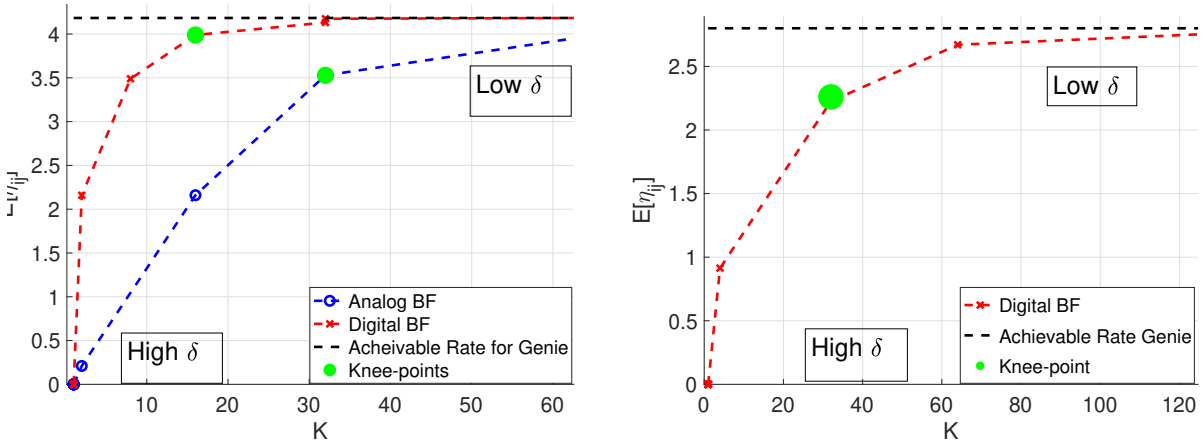

(a) 28 GHz

(b) 140 GHz

Fig. 10: Pareto boundaries for analog and digital beamforming at 28 and 140 GHz. We see that the 28 GHz system achieves a peak spectral efficiency of 4.2 bps/Hz, which reduces to 2.8 bps/Hz for 140 GHz. This is due to the higher blockage and reflection loss at sub-THz frequencies.

The choice of δ determines the operating point on the Pareto boundary of the power-throughput trade-off curve, which is shown for analog and digital beamforming at 28 and 140 GHz in Fig. 10 for $P_o = 99\%$. The curve corresponding to analog beamforming at 140 GHz is missing in Fig. 10b, since the optimization problem in (12)-(13) is infeasible for this case for $P_o = 99\%$, as seen in Fig. 7. The trade-off at the feasible 'knee-points' are presented in Table VI.

Beamforming/ Frequency	**Knee Point** K	**Power Saved (relative to** $K = N_{\mathrm{SSB}}$**)**	**Achieved Throughput (relative to Genie)**	**Power Consumed (mW)**
Analog/ 28 GHz	32	50 %	85 %	12.48
Digital/ 28 GHz	16	75 %	95 %	2.72
Analog/ 140 GHz	Optimization problem in (12)-(13) is in feasible for P_{o} = 99%.			
Digital/ 140 GHz	32	75 %	80 %	195.84

TABLE VI: Power-throughput trade-off at the knee points in Fig. 10.

D. Closeness to Optimality

While Fig. 10 provides an insight into the average throughput that can be achieved by the policies in Table V, it does not indicate how close their tracking performance approaches that of Genie. In Fig. 11, we plot the CDFs of $\gamma^{\pi}_{\mathrm{max}}$ corresponding to the knee points labelled in Fig. 10, along with the Genie CDF.

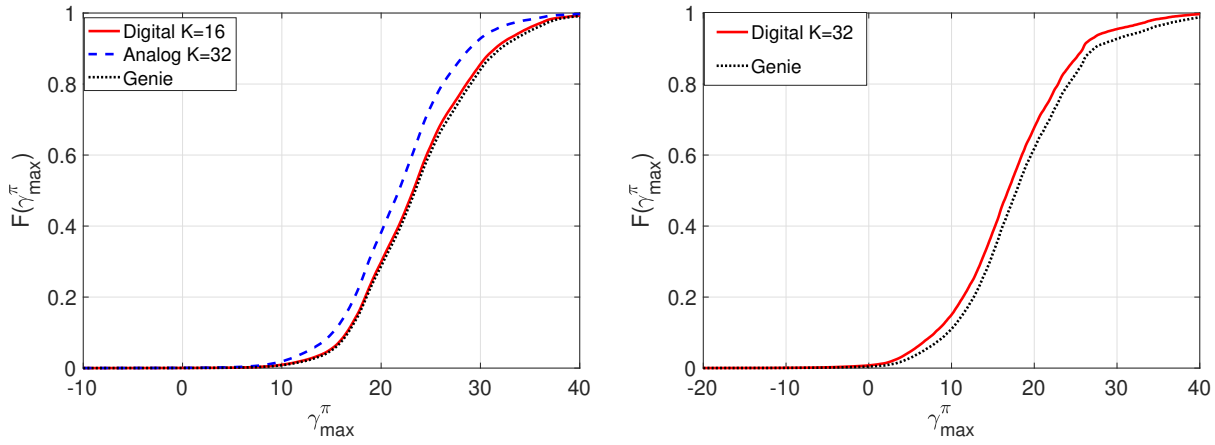

(a) 28 GHz

(b) 140 GHz

Fig. 11: Comparison of CDF of $\gamma^{\pi}_{\mathrm{max}}$ for awake time at knee points for digital and analog beamforming, with genie at 28 and 140 GHz

At 28 GHz, digital beamforming with $K = 16$ differs from Genie by only about 0.1 dB at 50-th percentile, while for analog beamforming with $K = 32$, the difference goes up to 2 dB. However, the power consumed by analog beamforming in this case exceeds that of digital

beamforming by a factor of 4.5, as shown in Table VI. At 140 GHz, the difference at the 50-th percentile is around 2dB for digital beamforming ($K = 32$).

E. Choice of Beamforming Architecture

From Table VI and Fig. 11, we observe that at 28 GHz, digital beamforming at the UE can save more power (relative to the corresponding maximum) and sacrifice less in terms of the throughput performance than analog beamforming, for an outage probability of at most 1%. The case for digital beamforming is even more compelling at 140 GHz, since none of our policies achieves an outage probability below 1% for analog beamforming, even in the absence of any power constraint. On the other hand, digital beamforming can save 75% power, while achieving 80% of the maximum throughput for an outage probability of at most 1%.

VII. Summary

DRX is likely to be aggressively used in mmWave and sub-THz wireless systems due to the high UE RFFE power consumption, which mainly stems from the need to track multiple links to ensure reliable multi-connectivity in the presence of frequent and severe link blockages. In this paper, we focused on reducing the UE power consumption during connected mode DRX by tracking only a subset of the available links, but without adversely affecting the outage/throughput performance. To achieve this objective, we formulated the choice of links to track over time as the outcome of a feasible policy for a MP-MAB problem. Through detailed system level simulations at 28 and 140 GHz, modeling a 5G and a hypothetical 6G system, respectively, we observed that even sub-optimal link tracking policies could achieve considerable power savings with relatively little degradation in outage and throughput performance, especially with digital beamforming at the UE.

Appendix A
Modeling UE RFFE Power Consumption

The UE RFFE components that contribute to the power terms on the right hand side of (1) are: (i) the Analog to Digital Converter(s) (ADCs), (ii) the Low Noise Amplifier(s) (LNAs), and (iii) the Local Oscillator (LO). We ignore the power consumption due to baseband processing

as the procedures in question are not processing intensive. Let $P_{\mathrm{ADC}}^{f_c,\mathrm{Analog}}$ and $P_{\mathrm{ADC}}^{f_c,\mathrm{Digital}}$ denote the power consumed by the ADC at carrier frequency f_c for analog and digital beamforming, respectively. Similarly, let $P_{\mathrm{LO}}^{f_c}$ and $P_{\mathrm{LNA}}^{f_c}$ denote the power consumed by the LOs and the LNAs, respectively.

From [10], the power consumed during the beam measurement (link tracking) procedure, $P_{\mathrm{BM}}^{f_c,\mathrm{BF}}$, is given by:

$$P_{\mathrm{BM}}^{f_c,\mathrm{BF}} = \begin{cases} \frac{KT_{\mathrm{SSB}}}{T_{\mathrm{SS}}}(P_{\mathrm{ADC}}^{f_c,\mathrm{Analog}} + P_{\mathrm{LO}}^{f_c} + P_{\mathrm{LNA}}^{f_c}), & \text{if BF = Analog} \\ N_{\mathrm{RX}}\frac{KT_{\mathrm{SSB}}}{T_{\mathrm{SS}}}(P_{\mathrm{ADC}}^{f_c,\mathrm{Digital}} + P_{\mathrm{LO}}^{f_c} + P_{\mathrm{LNA}}^{f_c}), & \text{if BF = Digital.} \end{cases} \tag{14}$$

We observe from (14) that $P_{\mathrm{BM}}^{f_c,\mathrm{BF}}$ has a linear dependence on K, which is proportional to the number of links tracked (see (3)). The additional N_{RX} factor for the digital beamforming case is a consequence of having N_{RX} RF chains. The power consumed during assignment listening, $P_{\mathrm{LS}}^{f_c,\mathrm{BF}}$, can be written as:

$$P_{\mathrm{LS}}^{f_c,\mathrm{BF}} = \begin{cases} \frac{T_{\mathrm{DRX,ON}}}{T_{\mathrm{DRX,Cyc}}}(P_{\mathrm{ADC}}^{f_c,\mathrm{Analog}} + P_{\mathrm{LO}}^{f_c} + P_{\mathrm{LNA}}^{f_c}), & \text{if BF = Analog} \\ \frac{T_{\mathrm{DRX,ON}}}{T_{\mathrm{DRX,Cyc}}}(P_{\mathrm{ADC}}^{f_c,\mathrm{Digital}} + P_{\mathrm{LO}}^{f_c} + P_{\mathrm{LNA}}^{f_c}), & \text{if BF = Digital,} \end{cases} \tag{15}$$

where $T_{\mathrm{DRX,ON}}$ is the DRX on time and $T_{\mathrm{DRX,Cyc}}$ is the DRX cycle time. Finally, the power consumed in beam reporting, $P_{\mathrm{BR}}^{f_c,\mathrm{BF}}$, is given by:

$$P_{\mathrm{BR}}^{f_c,\mathrm{BF}} = \begin{cases} \frac{2T_{\mathrm{sym}}}{T_{\mathrm{DRX,Cyc}}}(P_{\mathrm{ADC}}^{f_c,\mathrm{Analog}} + P_{\mathrm{LO}}^{f_c} + P_{\mathrm{LNA}}^{f_c}), & \text{if BF = Analog} \\ \frac{2T_{\mathrm{sym}}}{T_{\mathrm{DRX,Cyc}}}(P_{\mathrm{ADC}}^{f_c,\mathrm{Digital}} + P_{\mathrm{LO}}^{f_c} + P_{\mathrm{LNA}}^{f_c}), & \text{if BF = Digital,} \end{cases} \tag{16}$$

where T_{sym} is the OFDM symbol period.

The quantities in (14)-(16) depend on many system parameters that depend on f_c, which are chosen according to the 3GPP NR standard and listed in Table VII. For further details, we refer the reader to [10].

REFERENCES

[1] S. H. Ali Shah, S. Aditya, S. Dutta, C. Slezak, and S. Rangan, "Power Efficient Discontinuous Reception in THz and mmWave Wireless Systems," in *Proc. IEEE Intl. Workshop on Signal Processing Advances in Wireless Communications (SPAWC)*, July 2019, pp. 1–5.

[2] T. S. Rappaport, R. W. Heath Jr., R. C. Daniels, and J. N. Murdock, *Millimeter Wave Wireless Communications*. Pearson Education, 2014.

Parameter	**Value**		**Remarks**
Carrier frequency, f_c	28 GHz	140 GHz	
Occupied bandwidth, B (GHz)	0.400	1.6	We assume that B would scale roughly with f_c. Thus, relative to 28 GHz, we consider a $4\times$ increase in B at 140 GHz.
Sample rate (GHz)	0.491	1.966	The sample rate, which influences the ADC/DAC power consumption, depends on B and the FFT size; 28 GHz uses 4096 point FFT, while 140 GHz could use 2×4096 point FFT
Subcarrier spacing (SCS), kHz	120	240	SCS $= 120$ kHz and $B = 400$ MHz is common for early 5G deployments at 28 GHz [22]. The SCS is doubled at 140 GHz, since the bandwidth scales by a factor of 4, while the FFT size is only doubled.
OFDM symbol duration, T_{sym} (μs)	8.92	4.46	Derived from SCS [27].
No. of UE (gNB) antennas, N_{RX} (N_{TX})	8 (64)	64 (256)	The arrays sizes at 28 GHz are similar to previous capacity analyses [41], [50]. Assuming free space pathloss, $N_{\text{TX}}N_{\text{RX}} \propto f_c^2$ ensures a constant downlink power spectral density at both carrier frequencies, so that the data rate scales linearly with B. We consider a slightly larger scaling factor for $N_{\text{TX}}N_{\text{RX}}$ at 140 GHz - 32 instead of 25 - since (a) for a UPA at the UE with $\lambda/2$ element spacing, an eight-fold increase in N_{RX} results in a lower occupied chip area, and (b) a four-fold increase in N_{TX} is reasonable at the gNB.
Duration of one SSB, T_{SSB} (μs)	35.7	17.9	Equal to 4 OFDM symbols.
SSB burst period, T_{SS} (ms)	20	20	Default NR configuration [27].
Maximum no. of SSBs during an SSB burst period N_{SSB}	64	128	N_{SSB} has a maximum value of 64 for 5G NR systems for the default 120 KHz SCS [27]. The 240 kHz SCS at 140 GHz leads to a doubling of N_{SSB} [51].
DRX cycle time (ms), $T_{\text{DRX,Cyc}}$	5	5	From [52].
DRX on time (ms), $T_{\text{DRX,ON}}$	1/32	1/32	

TABLE VII: 3GPP NR based system parameters used to estimate the UE RFFE power consumption in connected mode DRX. Similar parameters are used in [10]

[3] T. S. Rappaport, S. Sun, R. Mayzus, H. Zhao, Y. Azar, K. Wang, G. N. Wong, J. K. Schulz, M. Samimi, and F. Gutierrez, "Millimeter wave mobile communications for 5G cellular: It will work!" *IEEE Access*, vol. 1, pp. 335–349, 2013.

[4] S. Rangan, T. S. Rappaport, and E. Erkip, "Millimeter-Wave Cellular Wireless Networks: Potentials and Challenges," *Proc. IEEE*, vol. 102, no. 3, pp. 366–385, 2014.

[5] S. Dutta, C. Barati, A. Dhananjay, D. A. Ramirez, J. F. Buckwalter, and S. Rangan, "A Case for Digital Beamforming at mmWave," *IEEE Trans. Wireless Commun.*, 2019.

[6] T. Kürner and S. Priebe, "Towards THz communications-status in research, standardization and regulation," *Journal of Infrared, Millimeter, and Terahertz Waves*, vol. 35, no. 1, pp. 53–62, 2014.

[7] I. F. Akyildiz, J. M. Jornet, and C. Han, "Terahertz band: Next frontier for wireless communications," *Physical Communication*, vol. 12, pp. 16–32, 2014.

[8] Y. Xing and T. S. Rappaport, "Propagation measurement system and approach at 140 GHz-moving to 6G and above 100 GHz," in *Proc. IEEE GLOBECOM*, 2018, pp. 1–6.

[9] M. Giordani, M. Polese, M. Mezzavilla, S. Rangan, and M. Zorzi, "Toward 6G networks: Use cases and technologies," *IEEE Communications Magazine*, vol. 58, no. 3, pp. 55–61, 2020.

[10] P. Skrimponis, S. Dutta, M. Mezzavilla, S. Rangan, S. H. Mirfarshbafan, C. Studer, J. Buckwalter, and M. Rodwell, "Power Consumption Analysis for Mobile mmwave and Sub-THz Receivers," in *2020 IEEE 6G Wireless Summit*, March 2020, pp. 1–5.

[11] J. Zhou, N. Nikaein, and T. Spyropoulos, "LTE/LTE-A discontinuous reception modeling for machine type communications," *IEEE Wireless Commun. Lett., vol. 2, no. 1, pp. 102-105*, 2013.

[12] H. Ramazanali, "Performance evaluation of LTE/LTE-a DRX: A Markovian approach," *IEEE Internet Things J., vol. 3, no. 3, pp. 386-397*, 2016.

[13] 3GPP, "TS 38.300, NR and NG-RAN Overall Description; Stage 2," 2017.

[14] ——, "TS 36.331 E-UTRA - Radio Resource Control (RRC) protocol specification - Release 13," 2016.

[15] M. K. Maheshwari, M. Agiwal, N. Saxena, and A. Roy, "Hybrid directional discontinuous reception (HD-DRX) for 5G communication," *IEEE Commun. Lett.*, vol. 21, no. 6, pp. 1421–1424, 2017.

[16] M. Agiwal, M. Maheshwari, N. Saxena, and A. Roy, "Directional-DRX for 5G wireless communications," *Electronics Letters*, vol. 52, no. 21, pp. 1816–1818, 2016.

[17] D. Liu, C. Wang, and L. K. Rasmussen, "Discontinuous Reception for Multiple-Beam Communication," *IEEE Access*, vol. 7, pp. 46 931–46 946, 2019.

[18] C. Slezak, V. Semkin, S. Andreev, Y. Koucheryavy, and S. Rangan, "Empirical Effects of Dynamic Human-Body Blockage in 60 GHz Communications," *IEEE Commun. Mag.*, vol. 56, no. 12, pp. 60–66, 2018.

[19] V. Raghavan, V. Podshivalov, J. Hulten, M. A. Tassoudji, A. Sampath, O. H. Koymen, and J. Li, "Spatio-Temporal Impact of Hand and Body Blockage for Millimeter-Wave User Equipment Design at 28 GHz," *IEEE Commun. Mag.*, vol. 56, no. 12, pp. 46–52, 2018.

[20] G. R. MacCartney, T. S. Rappaport, and S. Rangan, "Rapid fading due to human blockage in pedestrian crowds at 5G millimeter-wave frequencies," in *Proc. IEEE GLOBECOM*, 2017, pp. 1–7.

[21] J. Choi, "On the macro diversity with multiple BSs to mitigate blockage in millimeter-wave communications," *IEEE Commun. Lett.*, vol. 18, no. 9, pp. 1653–1656, 2014.

[22] M. Shafi, A. F. Molisch, P. J. Smith, T. Haustein, P. Zhu, P. De Silva, F. Tufvesson, A. Benjebbour, and G. Wunder, "5G: A tutorial overview of standards, trials, challenges, deployment, and practice," *IEEE J. Sel. Areas Commun.*, vol. 35, no. 6, pp. 1201–1221, 2017.

[23] D. Corcoran, L. Andimeh, A. Ermedahl, P. Kreuger, and C. Schulte, "Data driven selection of DRX for energy efficient 5G RAN," in *2017 13th Intl. Conf. on Netw. and Service Manag. (CNSM)*, 2017, pp. 1–9.

[24] L. Sharma, B. B. Kumar, and S. Wu, "Performance Analysis and Adaptive DRX Scheme for Dual Connectivity," *IEEE Internet Things J.*, vol. 6, no. 6, pp. 10 289–10 304, 2019.

[25] A. Alkhateeb, G. Leus, and R. W. Heath, "Compressed sensing based multi-user millimeter wave systems: How many measurements are needed?" in *Proc. IEEE Intl. Conf. on Acoust., Speech, Signal Process. Processing (ICASSP)*. IEEE, 2015, pp. 2909–2913.

[26] Z. Xiao, T. He, P. Xia, and X.-G. Xia, "Hierarchical codebook design for beamforming training in millimeter-wave communication," *IEEE Trans. Wireless Commun.*, vol. 15, no. 5, pp. 3380–3392, 2016.

[27] M. Giordani, M. Polese, A. Roy, D. Castor, and M. Zorzi, "A Tutorial on Beam Management for 3GPP NR at mmWave Frequencies," *IEEE Commun. Surveys Tuts.*, 2018.

[28] G. Yuan, X. Zhang, W. Wang, and Y. Yang, "Carrier aggregation for LTE-advanced mobile communication systems," *IEEE Commun. Mag.*, vol. 48, no. 2, pp. 88–93, 2010.

[29] Z. Shen, A. Papasakellariou, J. Montojo, D. Gerstenberger, and F. Xu, "Overview of 3GPP LTE-advanced carrier aggregation for 4G wireless communications," *IEEE Commun. Mag.*, vol. 50, no. 2, pp. 122–130, 2012.

[30] J. Singh, O. Dabeer, and U. Madhow, "On the limits of communication with low-precision analog-to-digital conversion at the receiver," *IEEE Trans. Commun.*, vol. 57, no. 12, pp. 3629–3639, 2009.

[31] V. Kuleshov and D. Precup, "Algorithms for multi-armed bandit problems," *Journal of Machine Learning Research*, vol. 1, 02 2014.

[32] Y. Zhou, J. Zhu, and J. Zhuo, "Racing Thompson: an Efficient Algorithm for Thompson Sampling with Non-conjugate Priors," in *Proc. Intl. Conf. on Machine Learning*, 2018, pp. 6000–6008. [Online]. Available: http://proceedings.mlr.press/v80/zhou18e.html

[33] Y. Gai, B. Krishnamachari, and R. Jain, "Combinatorial Network Optimization With Unknown Variables: Multi-Armed Bandits With Linear Rewards and Individual Observations," *IEEE/ACM Trans. Netw.*, vol. 20, no. 5, pp. 1466–1478, 2012.

[34] V. Va and R. W. Heath, "Basic Relationship between Channel Coherence Time and Beamwidth in Vehicular Channels," in *Proc. IEEE Veh. Technol. Conf. (VTC-Fall)*, Sep. 2015, pp. 1–5.

[35] 3GPP, "TR 38.901, Study on Channel Model for Frequencies From 0.5 to 100 GHz (Release 15) document," Jun. 2018.

[36] V. Raghavan, A. Partyka, A. Sampath, S. Subramanian, O. H. Koymen, K. Ravid, J. Cezanne, K. Mukkavilli, and J. Li, "Millimeter-wave MIMO prototype: Measurements and experimental results," *IEEE Commun. Mag.*, vol. 56, no. 1, pp. 202–209, 2018.

[37] T. Bai, R. Vaze, and R. W. Heath, "Analysis of Blockage Effects on Urban Cellular Networks," *IEEE Trans. Wireless Commun.*, vol. 13, no. 9, pp. 5070–5083, Sep. 2014.

[38] METIS, "METIS Channel Model, Tech. Rep. METIS2020, Deliverable D1.4 v3." 2015. [Online]. Available: https://www.metis2020.com/wp-content/uploads/deliverables/METIS D1.4 v1.0.pdf

[39] G. Maccartney, S. Deng, S. Sun, and T. Rappaport, "Millimeter-Wave Human Blockage at 73 GHz with a Simple Double Knife-Edge Diffraction Model and Extension for Directional Antennas," in *Proc. IEEE Veh. Technol. Conf. (VTC-Fall)*, 07 2016.

[40] 3GPP, "Study on channel model for frequencies from 0.5 to 100 GHz," TR 38.901 (release 14), 2018.

[41] M. R. Akdeniz, Y. Liu, M. K. Samimi, S. Sun, S. Rangan, T. S. Rappaport, and E. Erkip, "Millimeter wave channel modeling and cellular capacity evaluation," *IEEE J. Sel. Areas Commun.*, vol. 32, no. 6, pp. 1164–1179, 2014.

[42] Y. Xing, O. Kanhere, S. Ju, and T. S. Rappaport, "Indoor Wireless Channel Properties at Millimeter Wave and Sub-Terahertz Frequencies," in *Proc. IEEE GLOBECOM*, 2019, pp. 1–6.

[43] E. Hyytia, H. Koskinen, P. Lassila, A. Penttinen, J. Virtamo, and J. Roszik, "Random Waypoint Model in Wireless Networks," *Networks and Algorithms: Complexity in physics and Computer Science*, June 2005.

[44] I. K. Jain, R. Kumar, and S. Panwar, "Limited by capacity or blockage? a millimeter wave blockage analysis," *Proc. Intl. Teletraffic Congress*, pp. 153–159, 2018.

[45] 3GPP, "TR 38.214,, NR - Physical layer procedures for data - (release 15) document," Jun. 2018.

[46] ——, "TR 38.900,study on channel model for frequency spectrum above 6 GHz release," Jun. 2018.

[47] L. Liu, R. Downe, and J. Reid, "Multi-armed bandit strategies for non-stationary reward distributions and delayed feedback processes," *arXiv Prepr. arXiv1902.08593,*, vol. abs/1902.08593, 02 2019.

[48] 3GPP, "TS 38.214 E-UTRA - 5G NR Physical layer procedures for data - Release 15," 2018.

[49] P. Mogensen, W. Na, I. Kovacs, F. Frederiksen, A. Pokhariyal, K. Pedersen, T. Kolding, K. Hugl, and M. Kuusela, "LTE Capacity Compared to the Shannon Bound," in *Proc. IEEE Veh. Technol. Conf. (VTC-Spring)*, vol. 1, 05 2007, pp. 1234 – 1238.

[50] T. Bai, A. Alkhateeb, and R. W. Heath, "Coverage and capacity of millimeter-wave cellular networks," *IEEE Commun. Mag.*, vol. 52, no. 9, pp. 70–77, 2014.

[51] J. Campos, "Understanding the 5G NR Physical Layer," 2017.

[52] 3GPP, "3GPP TS 38.331. NR; Radio Resource Control (RRC) protocol specification," 2019.